

# Dense Nonaqueous Phase Liquid Architecture and Dissolution in Discretely Fractured Sandstone Blocks

CHARLES E. SCHAEFER,<sup>\*,†</sup>  
 AMY V. CALLAGHAN,<sup>†,‡</sup> JARED D. KING,<sup>§</sup>  
 AND JOHN E. MCCRAY<sup>§,||</sup>

Shaw Environmental, Inc., 17 Princess Road,  
 Lawrenceville, New Jersey 08648, and Environmental Science  
 and Engineering and Hydrologic Science and Engineering,  
 Colorado School of Mines, 1500 Illinois Street, Golden,  
 Colorado 80401

Received April 23, 2008. Revised manuscript received  
 December 30, 2008. Accepted January 7, 2009.

Laboratory experiments were performed in discretely fractured sandstone blocks to evaluate residual dense nonaqueous phase liquid (DNAPL) architecture and dissolution. Tetrachloroethene (PCE) DNAPL residual saturations (DNAPL volume/fracture volume) ranged between 0.18 and 0.52 for the rocks studied. DNAPL–water specific interfacial areas ranged between 19 and 57 cm<sup>2</sup>/cm<sup>3</sup>. No measurable correlation was observed between DNAPL–water interfacial area and aperture, aperture ratio, or residual saturation. DNAPL–water interfacial areas were comparable to those reported in sands with grain diameters similar to the rock apertures. However, the DNAPL residual saturation in the fractures were 2–4 times greater than in the sands, suggesting that PCE dissolution rates in rock fractures may be substantially less than in unconsolidated media, as the effective interfacial area per volume of DNAPL in rock fractures was less than in sands. Comparison of dissolution mass transfer coefficients in the bedrock fractures to corresponding mass transfer coefficients measured in sands indicated that dissolution rates in bedrock fractures were substantially less than dissolution rates measured in sands, even after normalization to DNAPL–water interfacial area. The presence of preferential water and DNAPL flow paths within the discrete fractures was shown to have a significant impact on observed DNAPL dissolution rates. DNAPL dissolution was reasonably described by a Reynolds number correlation that incorporated flow characteristics and the DNAPL–water interfacial area.

## Introduction

Groundwater contamination by dense nonaqueous phase liquids (DNAPLs) is a widespread environmental concern. Releases of chlorinated DNAPL compounds such as tetra-

chloroethene (PCE) may result in the downward migration of chlorinated solvents into fractured bedrock. DNAPL can become immobilized in bedrock fractures as a residual phase, where it can serve as a long-term contaminant source to groundwater and slowly diffuse (dissolved phase) into the rock matrix. The subsequent rate of DNAPL dissolution into surrounding groundwater is controlled by interfacial mass transfer between the DNAPL and groundwater, especially if groundwater velocities are high, as often is the case during implementation of a pump-and-treat remedial strategy, in fractured bedrock aquifers, and/or if there is a rapid reaction occurring near the DNAPL–water interface (e.g., in situ chemical oxidation).

The key parameters needed to evaluate and predict interfacial mass transfer between DNAPL and water in fractured geological settings are still not well understood because fundamental understanding regarding the configuration (i.e., DNAPL–water interfacial area) of dissolving DNAPL in bedrock fractures is lacking. Theoretical predictions (1–4) and experimental measurements (5–9) of fluid–fluid interfacial areas and DNAPL dissolution have been performed for unconsolidated media. These studies have provided insight into DNAPL configuration and morphology in sands and soils. The referenced DNAPL dissolution studies have generally shown that dissolution flux is proportional to the DNAPL–water interfacial area.

While recent studies (9) have measured the interfacial area and developed correlations for predicting an interfacial mass transfer coefficient in unconsolidated media, there is a notable absence of any similar studies (simultaneously measuring interfacial area and DNAPL dissolution) that have been performed for bedrock or fractured systems. Dickson and Thomson (10) performed DNAPL dissolution experiments in fractures and developed a fracture dissolution model to simulate dissolution of DNAPL in bedrock fractures. They note that their model is sensitive to a morphology index, which represents the ratio of DNAPL–water interfacial area to DNAPL volume. Similarly, simulations performed by Detwiler et al. (11) have shown that dissolution of nonaqueous phases in fractures is a function not simply of entrapped saturation but also of the geometry of the entrapped phase (i.e., DNAPL–water interfacial area). Simulations performed by Rubin et al. (12) also confirm the need to understand the interfacial mass transfer coefficient for NAPL dissolution in fractured bedrock. Thus, these studies identify the need to measure and evaluate DNAPL–water interfacial area in bedrock fractures in order to evaluate and predict DNAPL dissolution. However, to the best of our knowledge, comprehensive studies have not been carried out to evaluate DNAPL–water interfacial area, DNAPL dissolution rates, and DNAPL morphology in fractured bedrock systems.

The objective of this study was to evaluate relationships between DNAPL architecture and rate-limited dissolution in bedrock fractures. Specifically, DNAPL–water interfacial areas were measured and interfacial mass transfer coefficients were calculated as a function of water velocity in fracture flow experiments conducted in discretely fractured bedrock blocks.

## Experimental Section

**Materials.** Two sandstone types, termed Colorado Red and Arizona Buff, were obtained in 29 cm × 29 cm × 5 cm blocks from a commercial distributor in Golden, CO (Foothills Stone Co.). Two blocks of each sandstone type were used for the bedrock fracture experiments. Both rocks contained mineral bedding planes, which could be clearly observed along the

\* Corresponding author phone: 609-895-5372; fax: 609-895-1858; e-mail: charles.schaefer@shawgrp.com.

† Shaw Environmental, Inc.

‡ Present address: Department of Botany and Microbiology, University of Oklahoma, Norman, OK 73019.

§ Environmental Science and Engineering, Colorado School of Mines.

|| Hydrologic Science and Engineering, Colorado School of Mines.

rock edges. The rock matrix porosity, which was calculated by measuring the water uptake into small (11.5 cm × 5 cm × 1 cm) pieces of oven-dried rock until equilibrium was established, was approximately 15% for each rock.

An artificial groundwater was used in all experiments, which was prepared in the laboratory from deionized water amended with the following reagent-grade chemicals purchased from Sigma–Aldrich (St. Louis, MO): 180 mg/L NaSO<sub>4</sub>, 113 mg/L NaCl, 40 mg/L NaHCO<sub>3</sub>, 1.0 mg/L MnSO<sub>4</sub>·H<sub>2</sub>O, and HCl for a final pH of approximately 7.0. Sodium dodecyl benzenesulfonate (SDBS) was the anionic surfactant used as an interfacial tracer (Sigma–Aldrich). PCE was purchased from Sigma–Aldrich (St. Louis, MO), and sodium bromide was purchased from Fisher Scientific (Pittsburgh, PA).

**Batch Experiments.** Preliminary batch experiments were performed to determine whether substantial sorption and/or chemical interactions between dissolved PCE, SDBS, or bromide and the rocks were occurring. Approximately 10 g of crushed (<5 mm diameter) rock and 25 mL of artificial groundwater were added to 40-mL glass serum bottles. Controls without rock material also were prepared. PCE, SDBS, and sodium bromide were amended for final concentrations of 50, 10, and 100 mg/L, respectively. Samples were prepared in triplicate. After the samples were gently shaken on an orbital shaker at room temperature for 24 h (72 h for bromide), the aqueous phase was analyzed for SDBS, PCE, and bromide. Additional experiments also were performed in duplicate by placing 1-cm-thick slabs (approximately 45 cm<sup>2</sup>) of each rock in bromide solutions for a minimum of 2 weeks and then measuring the mass of bromide that diffused out of the rock into bromide-free water.

**Construction and Characterization of Fracture Systems.** Our approach for constructing laboratory-scale fracture systems was to induce a single fracture along the naturally occurring mineral bedding planes of the sandstone blocks. A 4-in.-wide masonry chisel was used to lightly tap along mineral bedding planes that were visible along the edges of the sandstone blocks. This light tapping induced a distinct fracture to occur along a natural bedding plane, causing the rocks to spontaneously split along the targeted bedding plane. Two fractured blocks of each type of sandstone were constructed. The interiors of the fractured Colorado and Arizona sandstones, showing the “top” and “bottom” of the horizontal fracture plane for each of the four rocks, are presented in the Supporting Information (Figure S1). The fracture surface was very irregular, creating an uneven fracture surface that mimicked the naturally occurring bedding planes. The fracture procedure yielded similar results for each rock, but the fracture surface of the Arizona sandstone was visually observed to be less rough and more uniform than that of the Colorado sandstone.

The methodology for creating discrete fracture systems for evaluating DNAPL dissolution was based on the general design and approach of Dickson and Thomson (10). A picture of the completed system for one of the Arizona rocks is shown in the Supporting Information (Figure S2). The two no-flow boundaries along the sides of the rock were sealed with Devcon plastic steel liquid (Grainger, Robbinsville, NJ). To prevent evaporative losses, the top and bottom of the rock were sealed with galvanized sheet metal that was attached with additional Devcon plastic steel putty. Small holes (0.20 cm) were drilled approximately 5 mm into the rock along the influent and effluent sides of the fracture. Pressurized air was applied to remove the resulting dust.

All wetted parts of the experimental system, including influent and effluent manifolds, were constructed with inert materials (i.e., stainless steel, Teflon, Kynar) that would not interact with PCE. The plastic female luer fittings of stainless steel needles (16G) were removed prior to inserting the needle bevels into the drilled holes. Care was taken to ensure that

the needles did not increase the fracture aperture. Twelve needles were inserted into the influent side of the rock, and 28 needles were inserted into the effluent side.

Plastic steel putty was used to seal the space around the needles and along the length of the fracture. Pieces of Teflon-lined ultra-chemical-resistant tygon tubing (0.16 cm i.d.) were attached to the blunt ends of the needles to serve as influent/effluent manifolds. Thus, the rate and distribution of water flow across the influent manifold into the fracture were based upon the “natural” permeability distribution of the bedrock fracture. The effluent lines were connected to two Teflon manifolds (AutoMate Scientific, Berkeley, CA). The manifolds were connected via Teflon tubing to a Y-fitting to facilitate effluent sampling. Based on the calculated volume of the fracture (presented in the Results and Discussion section) and the internal volume of the manifold, the residence time in the effluent manifold was less than 6% of the residence time in the fracture. The influent lines were connected to a high-precision/high-pressure piston pump (Cole-Parmer, Vernon Hills, IL) equipped with a high-resolution flowmeter. All fracture blocks were leak-tested to verify the integrity of the sealant and fittings. Testing also was performed to verify that the pressure drop across each manifold was less than the pressure drop across the fracture.

Initial fracture flow experiments were performed to characterize the fracture for each of the four rocks (C1, C2, A1, and A2). All rocks were prewetted for several days to ensure that the rock matrix was water-saturated prior to initiation of fracture flow experiments. The pressure drop across each rock fracture at a given flow rate was measured with a manometer tube; this testing was performed to provide an estimate of fracture aperture (described in the Results and Discussion section). In addition, bromide and SDBS tracer tests were performed in the absence of PCE DNAPL for each rock to (i) verify that SDBS sorption to the rock was negligible, (ii) evaluate potential impacts of matrix diffusion on solute transport through the fracture plane, and (iii) determine fracture aperture. Influent bromide and SDBS concentrations were 20 and 50 mg/L, respectively. Influent lines were prepurged with tracer to limit residence time in the influent tubing prior to entry within the rock. Effluent samples were collected as a function of time and analyzed for each tracer. Tracer testing was typically performed at a flow rate of approximately 0.1 mL/min. Tracer experiments were performed at least in duplicate for each rock.

**Fracture Dissolution Experiments.** Residual PCE was attained in the fractures by injecting two fracture volumes of PCE through the manifold at a flow rate of approximately 1.1 mL/min. Displacement of water from the rock effluent typically ceased before one fracture volume of PCE had been delivered; water and PCE appeared to flow through the same effluent ports in each experiment. A minimum of two fracture volumes of artificial groundwater was then injected into the rock at a flow rate of approximately 1 mL/min to attain residual PCE saturation. PCE displacement from the rock typically ceased within one fracture volume of water injection. An additional two fracture volumes (minimum) of water were subsequently injected into the rock at a flow of approximately 10 mL/min (capillary number ~ 10<sup>-5</sup>) to ensure that all mobile PCE was displaced from the fracture and influent/effluent manifolds and to ensure that PCE would not be mobilized during the dissolution experiments.

The residual PCE volume for each experiment was measured volumetrically as the difference between the PCE volume injected into the rocks and the total volume of PCE DNAPL that was recovered from the effluent after each post-PCE water flood; only separate-phase PCE was considered, as the volume of dissolved PCE was insignificant compared to the nonaqueous phase volume. Evaluation of alternate PCE flooding sequences were not performed in this study;

thus results are limited to the PCE saturation history examined in these experiments.

After residual PCE saturation (defined as residual PCE volume divided by fracture volume) was attained for each rock, bromide and SDBS tracer tests (0.1 mL/min flow rate) were repeated for each rock. Following the tracer testing, PCE dissolution kinetics were evaluated by measuring the effluent PCE concentrations as a function of flow rate (ranging from approximately 0.1 to 3 mL/min). To ensure equilibrium conditions, a minimum of two fracture volumes of water (without SDBS) at each tested dissolution flow rate were allowed to flow through the rock before an effluent concentration was measured. Because of the relatively low solubility of PCE, PCE mass removal during the dissolution testing did not result in a significant reduction in the residual PCE DNAPL mass (<5%).

At the conclusion of the experiment, several fracture volumes of ethanol were injected into the fractures to displace and dissolve the residual PCE. PCE concentrations in the effluent ethanol solution were measured to determine the mass of PCE DNAPL in the fractures and to verify that the DNAPL had been removed prior to beginning additional experiments.

**Analytical.** Chlorinated ethenes were analyzed via gas chromatography (GC) with mass spectrometric (MS) detection (Agilent GC-5890/MS-5971). SDBS was analyzed on a GENESYS 2 UV-spectrophotometer, with SDBS absorption at approximately 235 nm. Bromide was analyzed via ion chromatography (Dionex DX-120, Sunnyvale, CA).

## Results and Discussion

**Batch Experiments.** Results of the preliminary batch testing showed that sorption/interaction of SDBS, PCE, and bromide to either the Colorado or Arizona sandstones was negligible (<5% of solute mass sorbed to the rock). There were no measurable differences in the concentrations between the controls and the rock-amended bottles. The mass of bromide released from the small rock slabs was equal (<5% difference in mass) to the mass of bromide equilibrated within the pore volume of the rock matrix, thereby confirming that adsorption of the bromide was negligible. Thus, bromide was considered a conservative tracer for the fracture experiments, and in the absence of residual PCE, SDBS was expected to migrate at the same rate as water.

**Calculation of Fracture Properties.** Typical bromide tracer elution curves for each rock type are shown in the Supporting Information (Figure S3a–e). Elution of the bromide was regressed to the one-dimensional advection–dispersion equation:

$$R \frac{\partial C}{\partial t} = D \frac{\partial^2 C}{\partial x^2} - v \frac{\partial C}{\partial x} \quad (1)$$

where  $R$  is the retardation factor (equal to 1 for SDBS if PCE DNAPL is absent and equal to 1 for bromide with or without PCE DNAPL present),  $C$  is the aqueous solute concentration (milligrams per cubic centimeter),  $t$  is the time (seconds) minus the approximate residence time in the manifolds,  $v$  is the linear water velocity (centimeters per second),  $D$  is the aqueous dispersion coefficient (square centimeters per second), and  $x$  is the distance along the line of flow (centimeters). Bromide elution data were regressed to the solution of eq 1 by use of the public domain software CXTFIT (13). Regression results show that the bromide elution is well-described by this model ( $R^2 > 0.97$ ) and that bromide mass transfer between the matrix and fracture does not have a substantial impact on bromide elution. SDBS, in experiments without residual PCE, coeluted with the bromide, with no measurable retardation. Thus, consistent with the batch testing, SDBS interactions with the rock surface were negligible.

TABLE 1. Fracture Properties for Each Rock

rock	$\delta_f$ (cm)	$\delta_{mb}$ (cm)	$\delta$	FV <sup>a</sup> (cm <sup>3</sup> )
C1	0.0074	0.038	0.19	31
C2	0.011	0.039	0.28	32
A1	0.0031	0.054	0.057	45
A2	0.0023	0.098	0.023	82

<sup>a</sup> FV is the mass balance fracture volume, which is calculated by multiplying  $\delta_{mb}$  by the measured length (29 cm) and width (29 cm) of the fracture block. Standard error for the fracture volume was  $\leq 6\%$ .

Results of the initial bromide tracer and hydraulic head experiments also were used to estimate fracture aperture. A friction loss aperture was calculated as follows (10, 14):

$$\delta_f = L \sqrt{\frac{12\mu}{\rho g l \Delta H t_m}} \quad (2)$$

where  $\delta_f$  is the friction-loss aperture (centimeters),  $L$  is the measured fracture length in the direction of flow (29 cm length of block),  $\mu$  is the water dynamic viscosity (grams per centimeter per second),  $\rho$  is the fluid density (grams per cubic centimeter),  $g$  is the gravitational constant (981 cm/s<sup>2</sup>),  $\Delta H$  is the pressure drop across the fracture (centimeters of H<sub>2</sub>O), and  $t_m$  is the mean residence time (seconds). Mean residence time was estimated by dividing the fracture length by the regressed velocity. A mass-balance aperture, calculated on the basis of the volumetric flow rate and mean residence time of the bromide tracers, provides an improved estimate of the mean aperture and is calculated as follows (10, 14):

$$\delta_{mb} = \frac{Q t_m}{LW} \quad (3)$$

where  $\delta_{mb}$  is the mass balance aperture (centimeters),  $Q$  is the measured volumetric flow rate (cubic centimeters per second), and  $W$  is the measured fracture width perpendicular to flow (29 cm block width). The mass-balance aperture is used to calculate the fracture volume, which is simply  $\delta_{mb}$  multiplied by  $LW$ .

The friction-loss aperture is controlled by small aperture regions, while the mass-balance aperture is controlled by large aperture regions (10, 14). The aperture ratio ( $\delta$ ), defined as the ratio of the friction-loss to mass-balance aperture, serves as a means to characterize a fracture plane in terms of an effective aperture distribution exposed to flow. Values of  $\delta$  approaching unity indicate uniformity of fracture aperture across the fracture plane.

Calculated fracture properties based on initial flow (no DNAPL) and tracer experiments are shown in Table 1. Values in Table 1 are average values calculated from flow and tracer experiments performed at least in duplicate; all replicate experiments for each rock were within 10% of the average values presented in Table 1. Fracture aperture values listed in Table 1 are in reasonable agreement with those measured in other laboratory and field studies (10, 15–17). Mass-balance apertures and fracture volumes for all four rocks are similar, although the fracture aperture and fracture volume for A2 were approximately 2 times larger than for the other rocks. The friction-loss apertures for the two Colorado rocks are approximately 3 times greater than those for the Arizona rocks, suggesting that flow through the Colorado rock fractures is less constricted or less controlled by flow through small apertures compared to the Arizona rock fractures. The aperture ratios for the Colorado rocks are also greater than the Arizona rocks, indicating that water flowing through the Colorado rocks experiences narrower aperture distributions than water flowing through the Arizona rocks. This result is

**TABLE 2. Residual Saturation and DNAPL–Water Interfacial Area Values Measured for Each Rock<sup>a</sup>**

rock	residual saturation (cm <sup>3</sup> /cm <sup>3</sup> )	DNAPL–water interfacial area (cm <sup>2</sup> /cm <sup>3</sup> )
C1	0.22/0.26	25/19 <sup>b</sup> /20
C2	0.22/0.18/0.22	55/43 <sup>b</sup> /45/51
A1	0.41/0.38/0.38	56/57
A2	0.52/0.38/0.38/0.45	20/20/9.1 <sup>c</sup> /21 <sup>d</sup>

<sup>a</sup> Values obtained for replicate experiments are shown. Except where noted, the flow rate was approximately 0.1 cm<sup>3</sup>/min. The calculated standard error of residual saturation for each computed value is <12%. The resulting calculated standard error of interfacial area is less than 28% for each computed value (calculation provided in Supporting Information). <sup>b</sup> Flow rate was approximately 0.06 cm<sup>3</sup>/min. <sup>c</sup> This value was considered an outlier and was not used to compute the average interfacial area value used in subsequent calculations. <sup>d</sup> Flow rate was approximately 0.5 cm<sup>3</sup>/min.

somewhat surprising, given the visibly rougher surface of the Colorado rocks compared to the Arizona rocks. As discussed in the following sections, this may be due to channeled flow within the Colorado rocks that limits water movement to a relatively small fraction of the overall fracture volume.

**DNAPL Residual Saturation and Architecture.** Table 2 reports the measured PCE residual saturation and PCE–water interfacial area for each rock. Results of replicate PCE-trapping experiments indicate that measured residual saturation values were reasonably repeatable. Residual saturation values range from 0.18 (C2) to 0.52 (A2). Residual saturation values are within the range reported by others in bench-scale fracture experiments (10, 17). Total fracture volumes (mass balance fracture volume plus residual PCE volume) measured in each rock after attainment of residual PCE saturations were approximately equal to the mass balance fracture volumes listed in Table 1 (which did not contain residual PCE), thereby confirming our measurements of rock fracture volumes.

The large residual saturation values in rocks A1 and A2, relative to rocks C1 and C2, are likely due to connectivity of large apertures within the fractures. Several simulations and experimental observations (17, 18) have shown that percolation of a nonwetting phase through fractures will occur primarily through large aperture regions. The connectivity of these large aperture regions, and the extent to which large aperture regions are interconnected via small aperture regions, will control the extent to which water is displaced during PCE flooding and the overall saturation of PCE within the fracture prior to water flooding. The relatively large aperture ratios for C1 and C2 suggest that flow through large aperture regions can occur with limited (compared to A1 and A2) entry into small aperture regions. Because the entry of PCE into small apertures is limited by capillary forces, water displacement and overall PCE saturation (prior to beginning the final water flood) in rocks C1 and C2 are less compared to rocks A1 and A2. This suggests that PCE migrated through discrete pathways within the fractures of the Colorado rocks (more so than in rocks A1 and A2), leaving the majority of the fracture water in place. This is consistent with PCE migration in rocks C1 and C2 occurring through discrete preferential flow pathways that occupied a relatively small fraction of the fracture volume. PCE flowing through A1 and A2 encountered a wider range of aperture regions than in C1 and C2. Consistent with this explanation, the data in Figure 1 show that both water displacement and residual PCE saturation in the rocks are related to the aperture ratio,

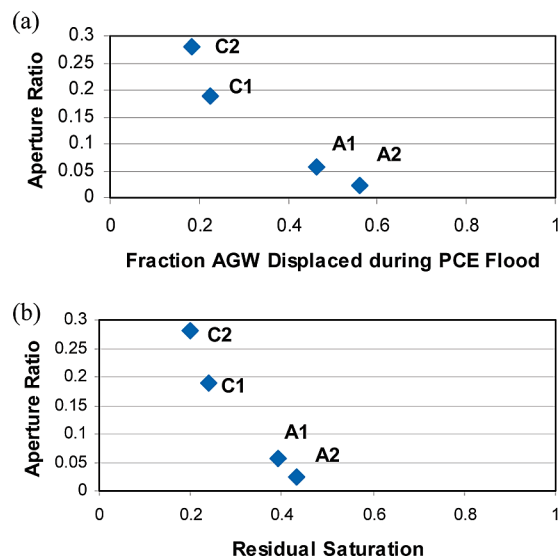


**FIGURE 1. Aperture ratio plotted as a function of (a) fraction of artificial groundwater (AGW) displaced during PCE flooding and (b) PCE residual saturation for each rock.**

and injection of PCE into the Colorado rocks was less dispersed (i.e., displaced less water) than the Arizona rocks.

Table 2 also lists the PCE–water interfacial area for each rock. PCE–water interfacial area was calculated by regressing (by use of CXTFIT)  $R$  in eq 1 to the SDBS elution data (values of  $D$  and  $V$  determined from the corresponding bromide tracer data; regressed values of  $R$  are provided in the Supporting Information) and applying the Gibbs adsorption equation as follows: (6, 19):

$$R = 1 + \frac{a_i K}{\theta} \quad (4)$$

$$K = \frac{\Gamma}{C} = \frac{M_w \partial \sigma}{R_g T \partial C} \quad (5)$$

where  $K$  is the sorption coefficient for SDBS at the PCE–water interface (cubic centimeters per square centimeter),  $a_i$  is the DNAPL–water interfacial area per fracture volume (square centimeters per cubic centimeter of fracture volume),  $\theta$  is the volumetric water content within the fracture (cubic centimeters per cubic centimeter),  $\Gamma$  is the SDBS mass sorbed at the PCE–water interface per unit interfacial area (milligrams per square centimeter),  $M_w$  is the SDBS molecular weight (milligrams per millimole),  $R_g$  is the gas constant (dyne centimeters per millimole per kelvin),  $T$  is temperature (kelvins), and  $\sigma$  is the PCE–water interfacial tension (dynes per centimeter). Equation 5 is evaluated at the influent SDBS concentration (50 mg/L). The slope of the interfacial tension versus SDBS concentration curve was determined by measuring the PCE–water interfacial tension as a function of SDBS concentrations by the pendant drop method (6, 20) and then regressing a polynomial expression to the data. Interfacial tension results are shown in the Supporting Information (Figure S4). No PCE was observed in the effluent during the tracer experiments; thus addition of surfactant and the relatively small reduction in interfacial tension did not result in any measurable DNAPL mobilization.

Measured PCE–water interfacial areas vary by approximately a factor of 2 among the four rocks, with no apparent correlation to the PCE residual saturation (Table 2). This observation suggests that the morphology of the residual PCE in effective contact with mobile water differs among the four rocks. It has been speculated that the aperture ratio is related to the DNAPL–water interfacial area and morphology

(10). However there is no observable correlation between fracture aperture and interfacial area for the rocks examined.

Karpyn et al. (17), using microcomputed tomography in Berea sandstone cores with a mean aperture of 0.058 cm, measured an oil–water interfacial area of 52 cm<sup>2</sup>/cm<sup>3</sup> at a residual saturation of 0.58; these measurements are reasonably consistent with values listed in Table 2. The interfacial area values in Table 2 also are comparable to DNAPL–water interfacial areas in sands with grain diameters similar to the rock apertures. Using a similar surfactant tracer method, Cho et al. (9) measured a DNAPL–water interfacial area of 44 cm<sup>2</sup>/cm<sup>3</sup> in sands with a 0.05-cm diameter. However, the residual DNAPL saturation in the sands was only 0.12, which is 2–4 times less than the residual saturations measured in the bedrock fractures. Saripalli et al. (19) measured a NAPL–water interfacial area of approximately 90 cm<sup>2</sup>/cm<sup>3</sup> in 0.025-cm diameter sand with a residual saturation of 0.22. Comparisons among these data suggest that the PCE–water interfacial area as a function of PCE residual saturation is greater in sands than in the Colorado and Arizona sandstones. This observation suggests that, for the rocks and sands studied, PCE dissolution rates in rock fractures may be substantially less than in unconsolidated media, as the effective interfacial area per volume of DNAPL in rock fractures is less than in sands.

As noted in Table 2, measured PCE–water interfacial areas did not appear to be sensitive to the flow rate of the SDBS tracer solution. If substantial PCE–water interfaces resided in aperture regions that were not contacted with mobile water (e.g., small aperture regions), then decreases in flow rate would likely result in an increase in the measured PCE–water interfacial area, as SDBS would have additional time to migrate to the PCE–water interfaces. Absence of this trend, for the flow rates examined, suggests equilibrium partitioning between surfactant and PCE–water interfaces in the fractures and that the PCE–water interfaces were well-contacted by mobile water regimes (21). Alternately, as discussed in the following section, multiple discrete flow paths within the fracture plane could exist. In this case, assuming that no measurable mixing occurred between the discrete flow paths, the above explanation would be applicable only to the discrete flow path(s) that contained PCE.

**DNAPL Dissolution.** Results of the DNAPL dissolution experiments for each rock are shown in Figure 2. PCE mass within the fractures remained relatively constant during the experiments, as less than 5% of the PCE mass was removed via dissolution. For all four rock experiments, effluent dissolved PCE concentrations approach equilibrium with decreasing flow velocity through the rock, which is consistent with dissolution results observed by others in unconsolidated media (9). These results indicate that PCE dissolution into the mobile water is mass-transfer-controlled and that equilibrium conditions are approached as the flow velocity through the fracture decreases. Equilibrium concentrations are approached more slowly in the Colorado rocks, especially for rock C1.

To explain this difference in dissolution behavior between the Colorado and Arizona rocks, we consider the DNAPL architecture. PCE in rocks C1 and C2 flowed through preferential pathways of large aperture regions and displaced very little water, as discussed in the previous section. After residual PCE saturation was attained, only a fraction of the water flow through the Colorado rocks likely came into contact with the residual PCE, as a substantial fraction of the water flowing through the rocks was in the “smaller” aperture regions in which PCE never entered. Thus, during dissolution in rocks C1 and C2, the net effluent PCE concentration is reduced due to dilution from flow paths that have not been contacted with PCE. Such flow heterogeneity would likely prevent effluent PCE concentrations in the C1 and C2 rocks from reaching equilibrium until velocities

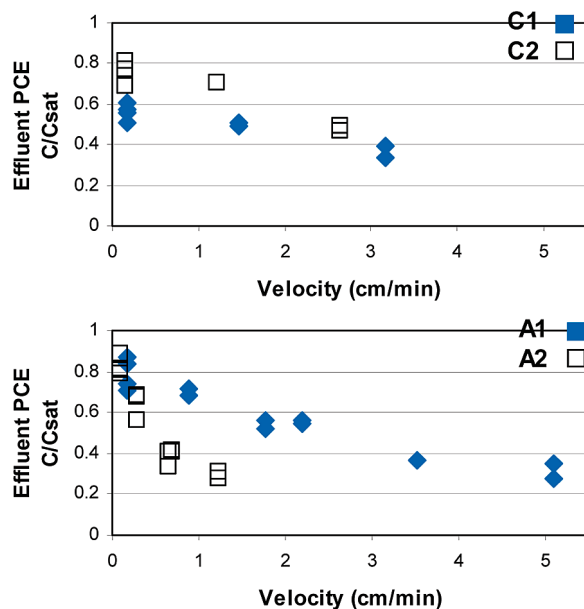


FIGURE 2. Effluent dissolved PCE concentration relative to PCE solubility, plotted as a function of water velocity for each rock.

decrease to very small values that would allow diffusion-controlled mixing across flow paths. Thus, fracture planes with preferential flow paths for DNAPL may have reduced dissolved contaminant concentrations relative to fracture planes with a more homogeneous flow field.

To further evaluate the dissolution data, lumped mass transfer coefficients were calculated by assuming (i) one-dimensional steady-state convection, dispersion, and dissolution in the fractures; (ii) a dissolved PCE concentration of zero at the fracture inlet; and (iii) a saturated PCE aqueous solution at infinite length (9, 22):

$$K_L = \frac{60\theta}{4D} \left[ \left( v - \frac{2D}{x} \ln \left( 1 - \frac{C}{C_{sat}} \right) \right)^2 - v^2 \right] \quad (6)$$

where  $K_L$  is the lumped mass transfer coefficient (converted to reciprocal minutes) and  $C_{sat}$  is the DNAPL aqueous solubility (milligrams per cubic centimeter). An intrinsic (or interfacial) mass transfer coefficient,  $K_i$  (centimeters per minute), is then calculated as follows:

$$K_i = \frac{K_L}{a_i} \quad (7)$$

Calculated values of  $K_L$  and  $K_i$  for each rock were evaluated as a function of the Reynolds number:

$$Re = \frac{\rho v \delta_f}{\mu} \quad (8)$$

where the friction-loss aperture is used as the characteristic length. This characteristic length was selected because it is assumed that DNAPL–water interfacial mass transfer will occur primarily where small aperture regions intersect large aperture regions (i.e., where DNAPL resides due to capillarity). As previously discussed, measurements of small aperture regions are better associated with the friction-loss aperture rather than the mass-balance aperture. Mass-transfer coefficients as a function of  $Re$  are plotted for each rock in Figure 3. In general, values of  $K_L$  and  $K_i$  increase nonlinearly with increasing  $Re$  and appear to approach an asymptotic value of  $K_L$  and  $K_i$  at higher  $Re$  values. This trend is likely due to higher velocities reducing the thickness of the boundary layer at the DNAPL–water interface, reducing diffusion lengths for mass transfer, and thus increasing the mass-transfer

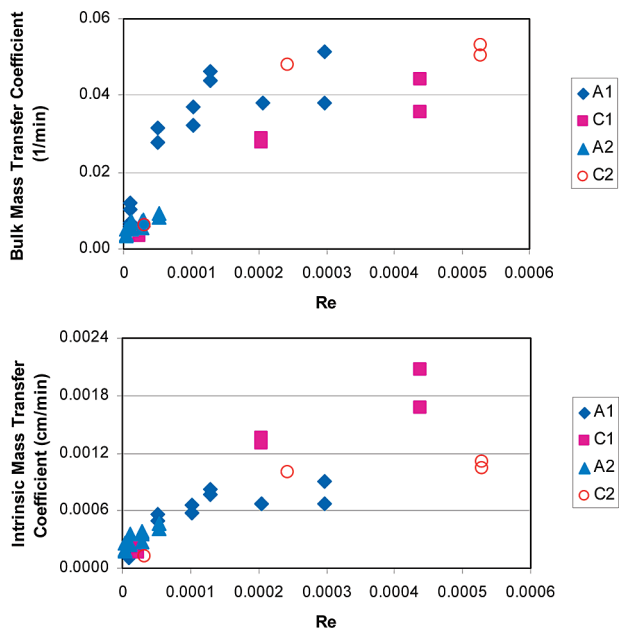


**FIGURE 3.** Lumped and intrinsic mass transfer coefficients, plotted as a function of Reynolds number for each rock.

coefficient. Results also indicate that the trends among the four rocks are more similar for  $K_L$  than for  $K_i$ . Thus, a reasonable correlation for the dissolution data among the four rocks as a function of flow can be attained by considering both the PCE–water interfacial area and the friction loss aperture.

By comparison, the lumped mass transfer coefficients measured by Dickson and Thomson (10) in limestone rock fractures at the start of dissolution were approximately 10 times less than those shown in Figure 3. DNAPL residual saturations attained by Dickson and Thomson ranged between 0.10 and 0.21, which were significantly less than those measured in the present study and may explain, in part, the discrepancy in dissolution kinetics between the two studies. The intrinsic mass transfer coefficients measured by Cho et al. (9) in sands were approximately 10 times greater than those shown in Figure 3. This comparison suggests that, even when DNAPL–water interfacial area is accounted for, DNAPL dissolution kinetics are substantially slower in the bedrock fracture planes than in sands, possibly due to decreased efficiency of mixing and mass transfer in fractures relative to unconsolidated media. As discussed in the previous section, the PCE–water interfacial area relative to the DNAPL residual saturation is larger in sands than in discrete bedrock fractures; thus, overall DNAPL dissolution rates in bedrock fractures is likely substantially less than the corresponding rate in unconsolidated sands. Further study with different rock types and fracture networks is needed to attain improved insight into DNAPL dissolution kinetics and morphology in fractured rock systems.

This study has shown that DNAPL dissolution rates in fractures are less than in unconsolidated media of comparable scale, suggesting that DNAPL dissolution in fractures is a relatively slow process compared to DNAPL dissolution in soils. The presence of preferential water and DNAPL flow paths, even within a single fracture plane, was shown to have a significant impact on observed DNAPL dissolution rates, which suggests that heterogeneity and DNAPL distribution at the fracture scale can impede dissolution processes. Examination of the DNAPL architecture relative to the fracture aperture and aperture distribution of the experimental systems was useful in evaluating PCE dissolution behavior. PCE dissolution was reasonably described by a Reynolds number correlation that incorporated DNAPL architecture

(friction loss aperture and DNAPL–water interfacial area). Development of this Reynolds number correlation and the insights attained into DNAPL dissolution in fractures could serve as useful tools in evaluating DNAPL dissolution in bedrock aquifers.

## Acknowledgments

Support for this research was provided in part by the Strategic Environmental Research and Development Program (SERDP) under Project ER-1554. We also thank Jonathan Myers for his assistance in statistical evaluations.

## Supporting Information Available

Four figures, showing inside views of fracture faces, experimental fracture system, bromide elution curves in rock, and PCE–water interfacial tension, and descriptions of regressed values of  $R$  from CXTFIT and error calculation for DNAPL–water interfacial area. This information is available free of charge via the Internet at <http://pubs.acs.org>.

## Literature Cited

- Held, R. J.; Celia, M. A. Modeling support of functional relationships between capillary pressure, saturation, interfacial area and common lines. *Adv. Water Resour.* **2001**, *24*, 325–343.
- Dillard, L. A.; Essaid, H. I.; Blunt, M. J. A functional relation for field-scale nonaqueous liquid dissolution developed using a pore network model. *J. Contam. Hydrol.* **2001**, *48*, 89–119.
- Dalla, E.; Hilpert, M.; Miller, C. T. Computation of the interfacial area for two-fluid porous medium systems. *J. Contam. Hydrol.* **2002**, *56*, 25–48.
- Clement, T. P.; Gautam, T. R.; Lee, K. K.; Truex, M. J.; Davis, G. B. Modeling coupled NAPL-dissolution and rate-limited sorption reactions in biologically active porous media. *Biorem. J.* **2004**, *8*, 47–64.
- Powers, S. E.; Abriola, L. M.; Weber, W. J. An experimental investigation of nonaqueous phase liquid dissolution in saturated subsurface systems: Transient mass transfer rates. *Water Resour. Res.* **1994**, *30*, 321–332.
- Schaefer, C. E.; DiCarlo, D. A.; Blunt, M. J. Determination of water-oil interfacial area during 3-phase gravity drainage in porous media. *J. Colloid Interface Sci.* **2000**, *221*, 308–312.
- Sahloul, N. A.; Ioannidis, M. A.; Chatzis, I. Dissolution of residual non-aqueous phase liquids in porous media: Pore scale mechanisms and mass transfer rates. *Adv. Water Resour.* **2002**, *25*, 33–49.
- Jeong, S. W.; Wood, A. L.; Lee, T. R. Enhanced removal of DNAPL trapped in porous media using simultaneous injection of cosolvent with air: Influencing factors and removal mechanisms. *J. Hazard. Mater.* **2003**, *101*, 109–122.
- Cho, J.; Annable, M. D.; Rao, P. S. C. Measured mass transfer coefficients in porous media using specific interfacial area. *Environ. Sci. Technol.* **2005**, *39*, 7883–7888.
- Dickson, S. E.; Thomson, N. R. Dissolution of entrapped DNAPLs in variable aperture fractures: Experimental data and empirical model. *Environ. Sci. Technol.* **2003**, *37*, 4128–4137.
- Detwiler, R. L.; Glass, R. J.; Rajaram, H. An investigation of the parameters controlling interphase mass transfer in variable aperture fractures. *Eos. Trans. AGU* **2002**, *83* (47), F496 (fall meeting supplement); Abstract H62G-08, 2002. American Geophysical Union Fall meeting, December 6–10, 2002, San Francisco, CA; UCRL-JC-149856-ABS.
- Rubin, H. K.; Rathfelder, K.; Abriola, L. M.; Spiller, M.; Köngeter, J. Using continuum approach to quantify the remediation of nonaqueous phase liquid contaminated fractured permeable formations. *J. Environ. Eng.* **2004**, *130*, 1345–1356.
- Toride, N.; Leij, F. J., van Genuchten, M. Th. The CXTFIT code for estimating transport parameters from laboratory or field tracer experiments. Research Report 137, U.S. Salinity Laboratory, Agricultural Research Service, Riverside, CA, 1995.
- Tsang, Y. W. Usage of ‘equivalent apertures’ for rock fractures as derived from hydraulic and tracer tests. *Water Resour. Res.* **1992**, *28*, 1451–1455.
- Cady, C. C.; Silliman, S. E.; Shaffern, E. Variation in aperture estimate ratios from hydraulic and tracer tests in a single fracture. *Water Resour. Res.* **1993**, *29*, 2975–2982.

- (16) Damste, J. S. S.; Schouten, S.; Keller, A. A. High resolution CAT imaging of fractures in consolidated materials. *Int. J. Rock Mech. Min. Sci.* **1997**, *34*, 358–370; Geomechanics Abstracts.
- (17) Karpyn, Z. T.; Grader, A. S.; Halleck, P. M. Visualization of fluid occupancy in a rough fracture using micro-tomography. *J. Colloid Interface Sci.* **2007**, *307*, 181–187.
- (18) Detwiler, R. L.; Rajaram, H.; Glass, R. J. Satiated relative permeability of variable-aperture fractures. *Phys. Rev. E* **2005**, *71*, 1–9.
- (19) Saripalli, K. P.; Rao, P. S. C.; Annable, M. D. Determination of specific NAPL-water interfacial areas of residual NAPLs in porous media using the interfacial tracers technique. *J. Contam. Hydrol.* **1998**, *30*, 375–391.
- (20) Anastasiadis, S. H.; Chen, J.-K.; Koberstein, J. T.; Seigel, A. F.; Sohn, J. E.; Emerson, J. A. The determination of interfacial tension by video image processing of pendant fluid drops. *J. Colloid Interface Sci.* **1987**, *119*, 55–66.
- (21) Jain, V.; Bryant, S.; Sharma, M. Influence of wettability and saturation on liquid-liquid interfacial area in porous media. *Environ. Sci. Technol.* **2002**, *37*, 584–591.
- (22) Morley, M. C.; Yamamoto, H.; Clausen, J. Dissolution kinetics of high explosives particles in a saturated sandy soil. *J. Contam. Hydrol.* **2006**, *85*, 141–158.

ES8011172